Report

TRANSPARENT PROCESS OPEN ACCESS

EMBO reports

Physiologically relevant miRNAs in mammalian oocytes are rare and highly abundant

Shubhangini Kataruka[1], Veronika Kinterova[2], Filip Horvat[1,3], Marcos Iuri Roos Kulmann[1], Jiri Kanka[2] & Petr Svoboda[1,*]

Abstract

miRNAs, ~22nt small RNAs associated with Argonaute (AGO) proteins, are important negative regulators of gene expression in mammalian cells. However, mammalian maternal miRNAs show negligible repressive activity and the miRNA pathway is dispensable for oocytes and maternal-to-zygotic transition. The stoichiometric hypothesis proposed that this is caused by dilution of maternal miRNAs during oocyte growth. As the dilution affects miRNAs but not mRNAs, it creates unfavorable miRNA:mRNA stoichiometry for efficient repression of cognate mRNAs. Here, we report that porcine *ssc-miR-205* and bovine *bta-miR-10b* are exceptional miRNAs, which resist the diluting effect of oocyte growth and can efficiently suppress gene expression. Additional analysis of *ssc-miR-205* shows that it has higher stability, reduces expression of endogenous targets, and contributes to the porcine oocyte-to-embryo transition. Consistent with the stoichiometric hypothesis, our results show that the endogenous miRNA pathway in mammalian oocytes is intact and that maternal miRNAs can efficiently suppress gene expression when a favorable miRNA:mRNA stoichiometry is established.

Keywords miR-10b; miR-205; miRNA; NanoLuc; oocyte
Subject Categories Development; RNA Biology
DOI 10.15252/embr.202153514 | Received 25 June 2021 | Revised 14 November 2021 | Accepted 16 November 2021 | Published online 6 December 2021
EMBO Reports (2022) 23: e53514

Introduction

MicroRNAs (miRNAs, reviewed in detail in Bartel (2018)) are genome-encoded ~22-nt-long single-strand small RNAs, which guide post-transcriptional repression of gene expression. A typical mammalian miRNA biogenesis (reviewed in Kim *et al* (2009)) involves nuclear processing of primary miRNA transcripts (pri-miRNA) into small hairpin precursors (pre-miRNA), which are transported to the cytoplasm. A cytoplasmic pre-miRNA is cleaved by RNase III Dicer, and a miRNA is loaded onto an Argonaute protein, the key protein component of the effector complex named RISC (RNA-induced silencing complex). Mammalian genomes encode four AGO proteins, which accommodate miRNAs equally well (Meister *et al*, 2004) and appear to be functionally redundant in the miRNA pathway (Su *et al*, 2009). However, AGO2 stands out among the mammalian AGO proteins, as it carries endonucleolytic activity cleaving cognate RNAs perfectly complementary to a loaded small RNA (Liu *et al*, 2004; Meister *et al*, 2004). AGO2 with a small RNA thus forms the minimal RISC (holo-RISC), which traditionally has been associated with the RNA interference pathway (Jinek & Doudna, 2009). While miRNAs guide RNAi-like endonucleolytic cleavage of perfectly complementary mRNAs by AGO2 as well (Hutvagner & Zamore, 2002; Yekta *et al*, 2004), a typical miRNA:mRNA interaction occurs through imperfect complementarity involving the "seed" region comprising nucleotides 2 to 8 of the miRNA (Brennecke *et al*, 2005; Sontheimer, 2005). Target repression through this type of interaction, referred to miRNA-like hereafter, is slower as it involves weaker and longer association of RISC with the target (Wee *et al*, 2012; Salomon *et al*, 2015). It also involves additional proteins, which form the full miRNA-loaded RISC (miRISC). The key AGO-binding partner is GW182 adaptor protein, which recruits further protein factors mediating translational repression coupled with deadenylation and decapping (Chekulaeva *et al*, 2011; Nishihara *et al*, 2013; Chen *et al*, 2014; Rouya *et al*, 2014).

miRNAs were implicated in countless physiological processes and pathologies. Thousands of mammalian miRNAs were annotated (Kozomara *et al*, 2019), and more than a half of mammalian genes could be directly targeted by miRNAs (Friedman *et al*, 2009). Yet, miRNAs are dispensable for mouse oocytes and preimplantation development and their activity in oocytes is negligible (Ma *et al*, 2010; Suh *et al*, 2010). Notably, analysis of miRNAs in mammalian oocytes revealed their low cytoplasmic concentration (<0.5 nM) (Kataruka *et al*, 2020) as opposed to functional miRNAs in somatic cells, which are relatively abundant (Bosson *et al*, 2014; Denzler *et al*, 2014, 2016). This is consistent with kinetic studies highlighting miRNA concentration as an important factor for efficient miRNA-mediated repression (Wee *et al*, 2012; Salomon *et al*, 2015). For example, analysis of *let-7* miRNA in HeLa cells, whose transcriptome size was estimated to be ~580,000 mRNA molecules/cell (Bishop *et al*, 1974), determined that a HeLa cell contains ~50,000

1 Institute of Molecular Genetics of the Czech Academy of Sciences, Prague 4, Czech Republic
2 Institute of Animal Physiology and Genetics of the Czech Academy of Sciences, Libĕchov, Czech Republic
3 Bioinformatics Group, Faculty of Science, University of Zagreb, Zagreb, Croatia
*Corresponding author. Tel: +420 241063147; E-mail: svobodap@img.cas.cz

© 2021 The Authors. Published under the terms of the CC BY NC ND 4.0 license

let-7 molecules (Bosson *et al*, 2014); this equals to ~20 nM cytoplasmic concentration (assuming ~20 μm cell diameter). In contrast, the cytoplasmic mRNA concentration in somatic cells and oocytes is comparable despite somatic cells containing 0.1–0.6 × 10^6 mRNA molecules while mouse oocytes accumulate a sizable transcriptome of ~27 × 10^6 mRNA molecules (Bishop *et al*, 1974; Hastie & Bishop, 1976; Piko & Clegg, 1982; Carter *et al*, 2005; Marinov *et al*, 2014; Fan *et al*, 2015). Maintenance of mRNA concentration in the cytoplasm in oocytes correlates with extended average half-life of maternal mRNAs (Jahn *et al*, 1976; Brower *et al*, 1981; De Leon *et al*, 1983), while turnover of maternal miRNAs does not appear to be adapted to the oocyte growth resulting in their dilution (Kataruka *et al*, 2020).

The "stoichiometric model" explaining the loss of physiologically significant activity of the miRNA pathway thus proposes that oocyte's growth dilutes maternal miRNA concentration to the point where miRNAs become ineffective regulators of the maternal transcriptome. Another explanation was offered by Freimer *et al* (2018) who proposed that alternative splicing of *Ago2* makes the functional AGO2 a limiting factor, which contributes to the observed miRNA inactivity. However, although this mouse-specific *Ago2* regulation could contribute to the negligible miRNA activity in mouse oocytes, it cannot explain low miRNA abundance and inactivity observed in bovine and porcine oocytes (Kataruka *et al*, 2020). Here, we report identification and analysis of two exceptionally abundant maternal miRNAs in bovine and porcine oocytes, which overcome the diluting effect, exhibit robust repressive activity, and support the stoichiometric model.

Results and Discussion

Extreme abundance of ssc-miR-205 and bta-miR-10b in oocytes

During analysis of published small RNA-sequencing (RNA-seq) data (Roovers *et al*, 2015; Gad *et al*, 2019), we noticed exceptional abundance and possible functional relevance of *ssc-miR-205* and *bta-miR-10b* in porcine and bovine oocytes, respectively (Fig 1A). Even though *miR-205* and *mir10b* are conserved across vertebrates (Lim *et al*, 2003), their high maternal expression is not conserved in mammals (Fig 1A). There are minimal sequence differences among the mouse, porcine, and bovine *miR-205* and *mir10b* miRNA precursors (Fig 1B). Consequently, the secondary structure of *ssc-miR-205* and *bta-miR-10b* precursors seems not associated with their high abundance in porcine and bovine oocytes, respectively (Figs 1B and EV1A).

Since RNA-seq data provided only relative estimates of miRNA abundance, we used quantitative RT–PCR to determine copy numbers per oocyte (Figs 1C and EV1C): *ssc-miR-205* was estimated to have ~1.6 million molecules per oocyte (~4.4 nM cytoplasmic concentration) and *bta-miR-10b* ~261,000 molecules per oocyte (~0.5 nM cytoplasmic concentration). Concentrations were estimated for 105 and 120 μm diameters of porcine and bovine oocytes, respectively (Griffin *et al*, 2006). In mouse oocytes, we have observed functional repression by miRNAs at 1.5 nM but not at 0.3 nM concentration (Kataruka *et al*, 2020). Thus endogenous *ssc-miR-205* would be predicted to suppress gene expression in oocytes, while repressive potential of *bta-miR-10b* was unclear.

Endogenous ssc-miR-205 and bta-miR-10b are active in oocytes

To estimate *ssc-miR-205* and *bta-miR-10b* activities in oocytes, we produced and microinjected luciferase reporters with perfectly complementary ("perfect"), partially complementary ("bulged" (Doench *et al*, 2003)), or mutated miRNA binding sites for *miR-205* or *miR-10b* (Fig EV2A). While artificial, bulged sites are a convenient counterpart of perfect sites used in reporters to partially distinguish between RNAi-like cleavage of the target and typical miRNA-mediated repression (Doench *et al*, 2003; Schmitter *et al*, 2006). Since the extensive 3' base pairing in bulged sites was associated with target-mediated miRNA degradation (TDMD, reviewed in Fuchs Wightman *et al*, 2018), we also produced a control reporter 4x-seed+suppl (Fig EV2B) where the four miRNA binding sites did not base-pair in the last five nucleotides, minimizing TDMD effects (Sheu-Gruttadauria *et al*, 2019).

Importantly, for miRNA-targeted reporters, we used NanoLuc luciferase (England *et al*, 2016), arguably the best tool for determining endogenous miRNA activity in oocytes. With the same miRNA binding sites as previously used in *Renilla* or firefly reporters, NanoLuc allows to reduce the reporter amount by an order of magnitude to approximately 10,000 reporter mRNA molecules per oocyte (Kataruka *et al*, 2020), which is well within the physiological range of maternal mRNA abundance (Fan *et al*, 2015).

Both miRNAs efficiently repressed all targeted reporters demonstrating that *ssc-miR-205* and *bta-miR-10b* are active and efficiently repressing targets (Figs 2A and EV2C). Consistent with its much higher abundance, *ssc-miR-205* in porcine oocytes attained much stronger reporter repression than *bta-miR-10b* in bovine oocytes (Fig 2A). These results provide strong evidence for efficient target repression by endogenous miRNAs in mammalian oocytes.

miRNA activities in mammalian oocytes do not appear to be suppressed in *sensu stricto*. The miRNA pathway appears mechanistically intact, but cytoplasmic miRNA concentrations are much lower than in somatic cells, and consequently, miRNA targets are repressed weakly. It is thus important that analysis of maternal miRNAs would respect physiological concentrations of miRNAs and their targets in order to avoid artifacts generated by non-physiological ones.

Several studies reported the presence of functional miRNAs in murine, bovine, or porcine oocytes (Chen *et al*, 2012; Sinha *et al*, 2017; Wang *et al*, 2017; Gad *et al*, 2020). In these studies, experimental support for significant endogenous miRNA activity in oocytes was inferred from correlative effects of miRNA overexpression or use of antisense inhibitory oligonucleotides ("antagomirs") (Krutzfeldt *et al*, 2005). For example, Chen *et al* reported that *miR-27a* activity is not suppressed in porcine oocytes (Chen *et al*, 2012). However, their functional analysis employed microinjection of oocytes with 50 pl of 500 ng/μl of miRNA mimics or inhibitors. That would correspond to more than a billion microinjected oligonucleotides, while an oocyte contains tens of millions of mRNA molecules (Fan *et al*, 2015). Similarly, *miR-98* function in mouse oocytes was studied using microinjection of 10 pl of 50 μM miRNA or 100 μM inhibitors (Wang *et al*, 2017). Since cytoplasmic volume of a mouse oocyte is ~260 pl, such experimental design would result in micromolar concentrations of microinjected oligonucleotides in the cytoplasm. This is three orders of magnitude or more than estimated amounts of maternal miRNAs (Kataruka *et al*, 2020) and an

 © 2021 The Authors

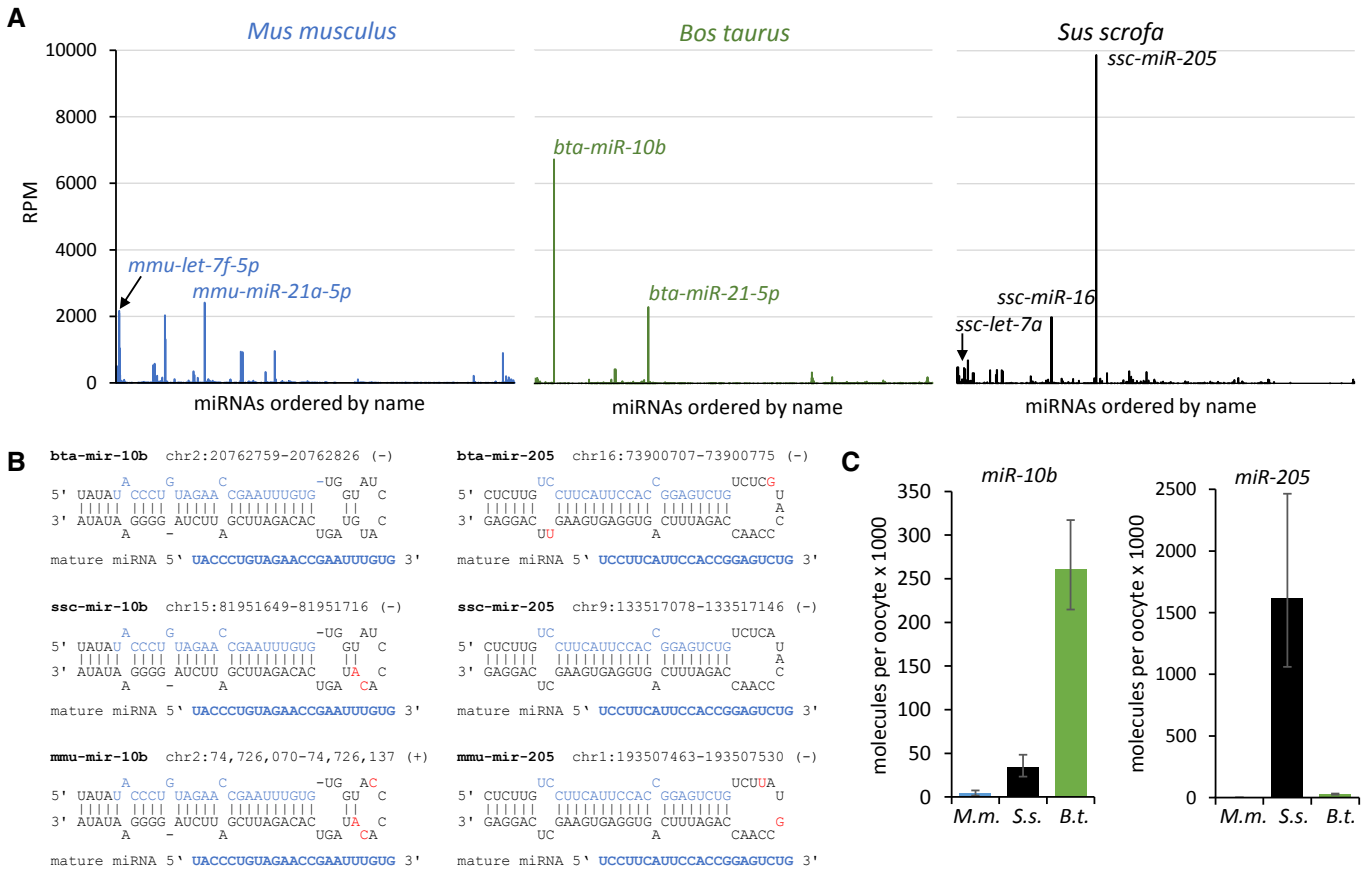

Figure 1. Most abundant miRNAs in mammalian oocytes.

A miRNA abundance in RNA-sequencing samples from murine, porcine, and bovine oocytes (Graf *et al*, 2014; Garcia-Lopez *et al*, 2015; Gad *et al*, 2019). Each graph shows on the *y*-axis reads per million of 19- to 32-nt reads for miRNAs and on the *x*-axis miRNAs ordered by name.

B Schematic depiction of miRNA precursors. Precursor sequences and predicted base pairing were adopted from miRbase miRNA annotations (Kozomara *et al*, 2019). *miR-10b* secondary structures in the miRBase contained two different base pairing versions in the loop, the alternative folding is displayed in Fig EV1A.

C qPCR quantification of *ssc-miR-205* and *bta-miR-10b* miRNAs in murine (*M.m.*), porcine (*S.s.*), and bovine (*B.t.*) oocytes, respectively. Shown are the mean values from three independent experiments. Error bars = SD. A detailed information concerning miRNA quantification is provided in the Methods section.

order of magnitude excess over the amount of maternal mRNAs (Fan *et al*, 2015). The analysis of *miR-130b* in bovine oocytes was conducted near the physiological range, as 10 pl of 50 nM miRNA or inhibitors was injected (Sinha *et al*, 2017). At the same time, this injected amount is higher than the amount of *bta-miR-10b*, the most abundant miRNA in bovine oocytes reported here, and there is no evidence that bta-*miR-130b* would reach similar abundance. In fact, miR-130b has three orders of magnitude lower abundance than miR-10b in RNA-seq from bovine oocytes (Roovers *et al*, 2015).

Endogenous ssc-miR-205 is biologically relevant

After determining the concentrations of *ssc-miR-205* and *bta-miR-10b* and assessing their activity, we focused on subsequent functional analysis of *ssc-miR-205*, which showed stronger target repression and because porcine oocytes were easily accessible for experimental analysis. To test whether *ssc-miR-205* suppresses endogenous targets, we inhibited the miRNA in the oocyte with *miR-205* antagomir microinjection and examined the mRNA levels of five selected predicted endogenous targets: *Plcb1*, *Prkab2*, *Lsm4*, *Mbip*, and *Srfbp1* by qPCR.

To test suppression of the endogenous targets, we microinjected fully grown transcriptionally quiescent porcine oocytes (Prather, 1993) with ~5 × 10^6 molecules of *miR-205* antagomir. This amount corresponds to ~two-fold excess over endogenous *ssc-miR-205* molecules and is much lower than amounts used to study miRNAs in oocytes in the studies mentioned above (Chen *et al*, 2012; Fan *et al*, 2015). Microinjected fully grown oocytes were cultured for 24 h in the presence of dbcAMP, which prevents resumption of meiosis (Appeltant *et al*, 2015). As the first wave of maternal mRNA degradation is induced during resumption of meiosis (Svoboda *et al*, 2015), the use of dbcAMP avoids interference of complex meiotic mRNA degradation with target degradation by miRNAs.

miR-205 antagomir caused a significant three-fold to five-fold increase in mRNA abundance for all predicted targets but not for two non-targeted control genes (Fig 2B). Derepression of the

© 2021 The Authors

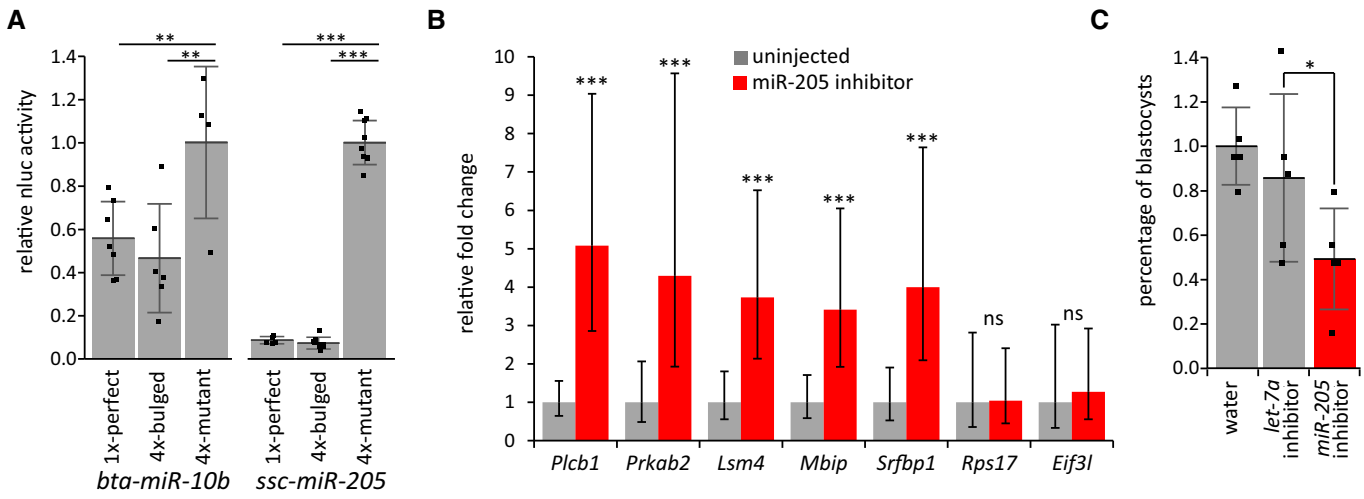

Figure 2. Endogenous miRNA activity is detected in bovine and porcine oocytes.

A *bta-miR-10b* and *ssc-miR-205* miRNAs efficiently repress microinjected NanoLuc luciferase reporters carrying a perfectly complementary (1× perfect) miRNA binding site or four partially complementary (4x-bulged) miRNA binding sites. See Fig EV2A for an overview of reporter design. Error bars = SD. Each data point represents a value obtained from five microinjected oocytes. Data were collected in two microinjection sessions, each microinjection session used a new batch of *in vitro*-transcribed reporter mRNAs.

B Derepression of predicted *ssc-miR-205* targets. In three independent microinjection experiments, *ssc-miR-205* was inhibited by a microinjected antisense oligonucleotide inhibitor and target levels were assessed 24 h after microinjection by RT–qPCR. Error bars = SD.

C Inhibition of *ssc-miR-205* by a microinjected antisense oligonucleotide inhibitor results in reduced development to the blastocyst stage. Shown is development of microinjected oocytes to the blastocyst stage relative to water-injected oocytes. Five independent experiments (represented by individual data points) were performed, ~50 porcine oocytes were microinjected in each group in each experiment. Difference between *let-7a* and *miR-205* inhibitor effects is statistically significant (two-tailed paired *t*-test *P*-value = 0.0169). Error bars = SD.

Data information: In panels A–C, asterisks indicate statistical significance (*P*-value) of one-tailed *t*-test (*$P < 0.05$, **$P < 0.01$, and ***$P < 0.001$).

endogenous targets upon injection of *miR-205* antagomirs complements results from NanoLuc reporter experiments and implies that *ssc-miR-205* is indeed functional in porcine oocytes and regulates endogenous gene expression in porcine oocytes.

Next, we examined whether *ssc-miR-205* plays a significant biological role in oocytes and/or early embryos. We microinjected fully grown porcine oocytes with the *miR-205* antagomir (~two-fold excess over endogenous *ssc-miR-205* molecules) and allowed them to undergo meiotic maturation, and then parthenogenetically activated their preimplantation development. We opted for parthenogenetic early development because porcine oocytes suffer a high incidence of polyspermy (Wang *et al*, 1994), while parthenogenotes can progress through the preimplantation development to the blastocyst stage (Hwang *et al*, 2020). As a negative control, we used *let-7a* inhibitor as this miRNA is present but not effective in porcine oocytes (Kataruka *et al*, 2020).

ssc-miR-205 inhibitor-injected oocytes showed ~50% reduced ability to support development to the blastocyst stage relative to water-injected control and *let-7a* inhibitor-injected oocytes (Fig 2C). The precise role of miR-205 inhibition in the phenotype remains unknown. There was no specific stage at which the development of *miR-205* antagomir-injected oocytes arrested and there are many predicted *ssc-miR-205* targets. The miRNA could play a role in shaping the zygotic expression or contribute to maternal mRNA degradation. Limitations of the model prevent determining whether *miR-205* antagomir-injected blastocysts would develop normally or show additional defects, similar to *miR-430* in zebrafish. *miR-430* is uniquely adapted for rapid and massive expression upon fertilization and contributes to maternal mRNA degradation in zebrafish embryos (Giraldez *et al*, 2006). Deletion of the *miR-430* cluster in zebrafish causes developmental delay and morphological defects at earlier developmental stages, while mutant embryos are able to undergo gastrulation and organogenesis before they die five days after fertilization (Liu *et al*, 2020). Thus, dissection of the biological role of *ssc-miR-205* in early porcine embryos will require further analysis of *ssc-miR-205* effects on maternal and zygotic transcriptomes to reveal the phenotype severity and strengthen the link between the phenotype and *ssc-miR-205* function.

High abundance of ssc-miR-205 correlates with its longer half-life

Exceptional abundance of *ssc-miR-205* in porcine oocytes suggests existence of one or more adaptations, which would be unique for *ssc-miR-205* in porcine oocytes and enable such a high accumulation of this miRNA during porcine oocyte growth. As mentioned above, there are minimal differences among the porcine, bovine, and murine miRNA precursors, which do not have any apparent effect on the secondary structure of the precursor (Fig 1B). This makes unique secondary structure or sequence variability of mature miRNA or miRNA* less likely explanations for *ssc-miR-205* accumulation.

Porcine oocyte-specific high abundance of *ssc-miR-205* could come from unusually high transcription of the miRNA precursor. RNA sequencing from porcine, bovine, and mouse oocytes (Graf

 © 2021 The Authors

et al, 2014; Garcia-Lopez *et al*, 2015; Roovers *et al*, 2015; Horvat *et al*, 2018; Gad *et al*, 2019; Jiao *et al*, 2020) suggests that *ssc-miR-205* is well expressed. However, transcription at the *ssc-miR-205* locus does not seem to be strikingly high (Fig 3). Porcine and bovine *miR-205* apparently originate from a nascent transcript of a spliced lncRNA (Fig 3). Production of the miR-205 pre-miRNA and splicing of the lncRNA are mutually exclusive because of an intron/exon boundary within the pre-miRNA (Fig 3). Albeit the boundary appears conserved in mice, RNA-seq data from oocytes and somatic tissues do not provide evidence for splicing of the *mmu-miR-205* host transcript (Abe *et al*, 2015; Veselovska *et al*, 2015; Sollner *et al*, 2017; Horvat *et al*, 2018) (Fig 3). Abundance of the porcine *miR-205* host lncRNA in oocytes is approximately twenty times higher than the *miR-205* host lncRNA level in bovine oocytes, but it still seems rather low (~3 CPM level, Fig 3) to explain production of 1.6 million *ssc-miR-205* molecules per oocyte. In comparison, highly abundant mRNAs such as *Zp3* and *Gdf9*, which would be expected to have hundreds of thousands of mRNA copies/oocyte, have expression around 700–800 CPM (Gad *et al*, 2019; Jiao *et al*, 2020).

Other porcine miRNA loci expressed in oocytes carry miRNAs in introns without apparent interference with splicing. These miRNAs show similar or even higher expression of spliced lncRNA precursor. For example, the *ssc-miR-16* locus produces the second most abundant maternal miRNA. The miRNA is localized in an intron of a spliced lncRNA, which has much higher abundance than the spliced lncRNA at the *ssc-miR-205* locus (Fig EV3A). A spliced ncRNA transcript from the *miR-17-92* cluster locus (also known as the "OncomiR" cluster (He *et al*, 2005)) is another lncRNA with abundance comparable to the *ssc-miR-205* locus lncRNA (~3 CPM level). However, relative to *ssc-miR-205*, the six miRNAs from the oncomir cluster had lower amounts with considerable variability among the oncomirs (Fig EV3B). Taken together, transcriptome analysis does not explain exceptionally high abundance of *ssc-miR-205* in oocytes. We cannot rule out that the precursor is exceptionally highly expressed, efficiently processed into mature miRNA while the host lncRNA is unstable and does not accumulate. However, we find it more likely that in addition to transcription other factors contribute to the observed *ssc-miR-205* abundance in oocytes.

We thus investigated whether *ssc-miR-205* accumulation could be also regulated at the level of the mature miRNA. We first examined decay of *ssc-miR-205* in fully grown oocyte since miRNA turnover appeared to be a contributing factor to miRNA dilution in mouse oocytes. We cultured transcriptionally quiescent fully grown oocytes for 10, 20, and 40 h. dbcAMP was added to the medium to prevent resumption of meiosis and maintain fully grown oocytes in the germinal vesicle stage during the experiment, so the changes in RNA metabolism, which are associated with meiotic maturation, would not affect the outcome of the experiment. We observed that *ssc-miR-205* exhibits higher stability than three other tested miRNAs, particularly *ssc-let-7a* (Fig 4A and B). *Let-7a* belongs to medium-to-high abundant miRNAs in porcine oocytes (Fig 1A) (Gad *et al*, 2019). While *ssc-let-7a* levels were reduced by ~70% over the course of 40 h (similar to mouse oocytes (Kataruka *et al*, 2020)), *ssc-miR-205* levels were reduced only by ~25% after 40 h (Fig 4A and B). Additional two examined miRNAs, *ssc-miR-10b* and *ssc-miR-22*, were less stable than *ssc-miR-205* but more stable than *ssc-let-7a*. These data suggest that increased miRNA stability could be one

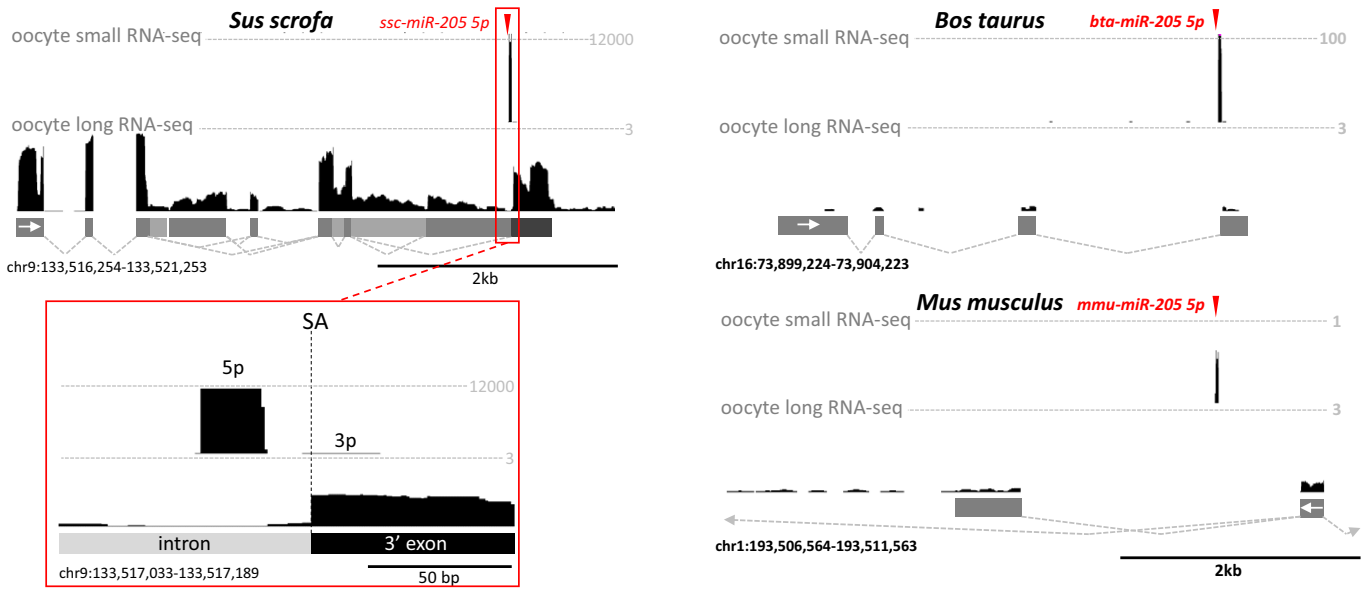

Figure 3. Transcription in the miR-205 miRNA locus from selected species.

UCSC browser snapshots show tracks from small and long RNA-seq analyses of mouse (Garcia-Lopez *et al*, 2015; Horvat *et al*, 2018), bovine (Graf *et al*, 2014; Roovers *et al*, 2015), and porcine oocytes (Gad *et al*, 2019; Jiao *et al*, 2020). Tracks were constructed as described in the Material and Methods. The y-scale for small RNAs depicts counts per million (CPM) of mapped 19- to 32-nt reads. The y-scale for long RNA-seq depicts CPM of mapped fragments. Gray rectangles and dashed lines represent exon–intron structure and transcript splicing inferred from RNA-seq data. Although the splice acceptor of the terminal exon appears conserved, murine RNA-seq data do not support splicing of the primary *miR-205* transcript. Instead, the *mmu-miR-205* locus produces a detectable antisense spliced maternal lncRNA while the precursor of *mmu-miR-205* is undetectable. SA, splice acceptor for the last exon of lncRNA originating from the locus.

© 2021 The Authors

factor contributing to accumulation of *ssc-miR-205* during oocyte growth.

The cause of increased stability of *ssc-miR-205* remains unclear, but it does not involve a 2'-OH modification of the miRNA, such as 2'-O-methylation, which is common for plant miRNAs and was reported to stabilize *miR-21-5p* in lung cancer (Liang *et al*, 2020). Endogenous *ssc-miR-205* and *bta-miR-10b* miRNAs vanished upon oxidation, suggesting that they do not carry 2'-O-methylation (Fig 4C). In contrast, no change was observed in the level of 2'-O-methylated *miR-221* oligonucleotide, which served as a positive control (Fig EV4B).

A well-established mechanism regulating mature miRNA turnover is non-templated nucleotide addition at their 3' end (Krol *et al*, 2010). Monoadenylation was reported to increase miRNA stability (D'Ambrogio *et al*, 2012) and is a common miRNA modification observed in mouse oocytes, but miRNA abundance and monoadenylation frequency do not correlate (Yang *et al*, 2016). We observed that 16.4% of *ssc-miR-205* in porcine oocytes was monoadenylated, which was more than the monoadenylation frequency observed in the next four abundant porcine miRNAs (Fig 4D). However, *bta-mir-10b*, the most abundant bovine oocyte miRNA, had lower monoadenylation level (4.6%) than less abundant *bta-miR-148* (10.7%) or *bta-miR-92a* (19.1%, Fig 4D). Thus, analysis of non-templated additions of five most abundant miRNAs in porcine, bovine, and murine oocytes showed inconclusively variable monoadenylation levels. Furthermore, while monoadenylation can contribute to *ssc-miR-205* accumulation, the *ssc-miR-205* monoadenylation could also be in part a consequence of high miRNA stability.

Another candidate mechanism for selective *ssc-miR-205* accumulation is interaction with some maternal RNA molecule, which would increase *ssc-miR-205* stability. Such an RNA could explain species-specific and tissue-specific *ssc-miR-205* accumulation in porcine oocytes. A precedent for such a regulation could be effect of circular RNA *Cdr1* on *miR-7* in the mouse brain (Piwecka *et al*, 2017). However, search for a putative binding partner among circRNAs, lncRNA, and mRNAs did not yield any outstanding candidate, which would have high abundance and multiple *ssc-miR-205* binding sites. The strongest candidate was a highly abundant

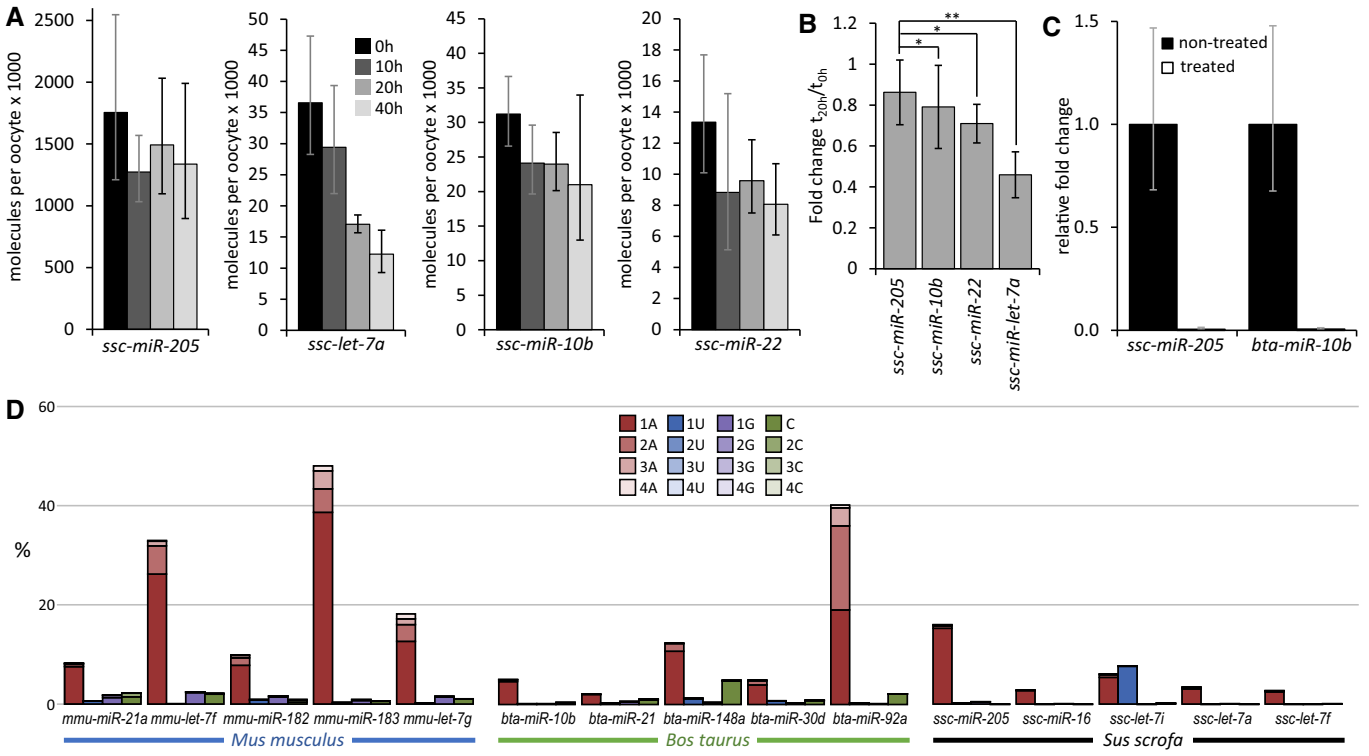

Figure 4. Selected features of *ssc-miR-205*.

A *ssc-miR-205* turnover. Fully grown transcriptionally quiescent oocytes were cultured for indicated periods of time, and selected miRNAs were quantified by RT–qPCR in four (*ssc-let-7a*), five (*ssc-miR-22*), or six (*ssc-mir10b* and *ssc-miR-205*) independent experiments. Error bars = SD.

B Comparison of mean relative changes of miRNA level at 20 h of culture (see Fig EV4A for 40 h data). *ssc-miR-205* in oocytes is less than *ssc-miR-10b*, *ssc-miR-22*, or ssc-let-7a. Error bars = SD. Asterisks indicate statistical significance (*P*-value) of one-tailed paired *t*-test (*$P < 0.05$, **$P < 0.01$).

C Treatment by sodium periodate followed by qPCR does not support 2'-OH modification of either *ssc-miR-205* or *bta-miR-10b* miRNA. Shown are relative levels of the sodium periodate-treated samples to non-treated samples, which were set to one. The experiment was performed three times. Error bars = SD. Efficiency of periodate treatment was confirmed using non-methylated and methylated miR-221 RNA oligonucleotides (EV4B).

D 3′ tailing of small RNAs in murine, bovine, and porcine oocytes (Graf *et al*, 2014; Garcia-Lopez *et al*, 2015; Gad *et al*, 2019). Shown are percentages of miRNAs tailed at 3′ end with mono- and oligonucleotides.

© 2021 The Authors

unspliced ~28-kb-long piRNA precursor RNA carrying several *miR-205* seed motifs. However, given the length of this RNA, it is hard to envision how this transcript could selectively stabilize *ssc-miR-205* and no other maternal miRNAs.

Taken together, we show that highly abundant maternal miRNAs *ssc-miR-205* and *bta-miR-10b* overcome the constraints imposed on miRNA activity by the size of the maternal transcriptome and volume of the oocyte. Our results support the model that the main cause of the apparent maternal miRNA inactivity is unfavorable miRNA:mRNA stoichiometry. In addition, we provide a framework for the identification of functionally relevant miRNAs in the oocyte. *ssc-miR-205* reported here is the best experimentally documented example of an active maternal mammalian miRNA, which functionally contributes to zygotic development. At the same time, the lack of conserved high abundance of *miR-205* and *miR-10b* in mammalian oocytes suggests that these two miRNAs represent unique evolutionary events. Thus, they are exceptions from the common biological insignificance of maternal miRNAs that did not adapt to the diluting effect of oocyte growth.

Materials and Methods

Oocyte collection and microinjection

Porcine and bovine oocytes were obtained from the slaughterhouse material as described previously (Blaha *et al*, 2015; Kinterova *et al*, 2019). For reporter injection, a mixture of *in vitro*-transcribed firefly and nanoluciferase (NanoLuc) RNA in the ratio of 100,000:10,000 was injected per oocyte with FemtoJet microinjector (Eppendorf). For antisense oligonucleotide inhibitor injection, commercially obtained hsa-let-7a-5p or hsa-miR-205-5p miRCURY LNA miRNA inhibitor (Qiagen, cat# YI04101776 and YI04101508, respectively) was diluted in water and microinjected (~5×10^6 molecules per oocytes).

Injected bovine oocytes were cultured in MPM media (prepared in-house (Kinterova *et al*, 2019)) containing 1 mM dbcAMP (Sigma) without a paraffin overlay in a humidified atmosphere at 39°C with 5% CO_2 for 20 h. Porcine oocytes were cultured in M-199 medium (Gibco) supplemented with 1 mM dbcAMP, 0.91 mM sodium pyruvate, 0.57 mM cysteine, 5.5 mM HEPES, antibiotics, and 5% fetal calf serum (Sigma). Injected oocytes were incubated at 38.5°C in a humidified atmosphere of 5% CO_2 for 20 h.

Parthenogenetic activation and embryo culture

After maturation, oocytes were washed twice in PXM-HEPES and activated by exposure to 10 μM ionomycin in PXM-HEPES for 5 min. This was followed by two washes in porcine zygote medium 3 (PZM 3) supplemented with 2 mM 6-DMAP and cultivation for 5 h at 38.5°C in 5% CO_2. Then, they were washed twice in PZM 3 and cultivated for seven more days in PZM 3 medium.

cDNA synthesis and qPCR

For miRNA analysis, oocytes were washed with M2 media to remove any residual dbcAMP, collected in a minimum amount of M2 media with 1 μl of RiboLock, and incubated at 85°C for 5 min to release the RNA. cDNA synthesis for miRNA analysis was done with the miRCURY LNA RT Kit (Qiagen, cat# 339340) according to the manufacturer's protocol. qPCR was set using cDNA fraction corresponding to one oocyte equivalent per qPCR. The miRCURY LNA SYBR Green Kit (Qiagen, cat# 339345) was used as per the manufacturer's protocol, and the reaction was set in Roche LightCycler 480. Each biological replicate was analyzed in a technical triplicate. The following primer sets from Qiagen were used: hsa-let-7a-5p (cat# YP00205727), hsa-miR-205-5p (cat# YP00204487), hsa-mir-10b-5p (cat# YP00205637), and hsa-mir-221-3p (cat# YP00204532). For miRNA quantification, a standard curve was produced using a *let-7a* oligonucleotide as described previously (Kataruka *et al*, 2020). A standard curve was also produced using a *miR-205* oligonucleotide (Fig EV1B) to assure that the *let-7a* oligonucleotide used in the previous work and here did not distort *ssc-miR-205* quantification. Comparison of quantifications showed that *miR-205* oligonucleotide-based calibration yielded slightly higher estimate of *ssc-miR-205* (1.91×10^6 molecules, Fig EV1C) than *let-7a* oligonucleotide-based calibration (1.62×10^6 molecules, Fig 1C). Thus, *let-7a* oligonucleotide-based calibration was used for data presentation to be consistent with the previous report (Kataruka *et al*, 2020).

For mRNA analysis, oocytes were washed and lysed for cDNA synthesis as for miRNA. Reverse transcription with Maxima Reverse Transcriptase (Thermo Scientific) was primed with random hexanucleotides. Maxima SYBR Green qPCR Master Mix (Thermo Scientific) was used for qPCR. qPCR was set using cDNA fraction corresponding to one oocyte equivalent per qPCR in technical triplicates for each biological sample (also in triplicates). Average CT values of the technical replicates were normalized to uninjected control oocytes.

Plasmid reporters

Nanoluciferase plasmid pNL1.1 was obtained from Promega. The Nluc gene was cleaved out and ligated in the phRL-SV40 plasmid downstream of the T7 promoter. miRNA binding sites were obtained as oligonucleotides from Sigma. Oligonucleotides were annealed, phosphorylated, and cloned downstream of the Nluc gene in XbaI site. The firefly control plasmid was made in-house with a T7 promoter (oligonucleotide sequences are provided in Table EV1).

In vitro transcription

Linearized pNL-miR-205 and miR-10b-perfect, bulged, mutant, and firefly plasmids were *in vitro*-transcribed, capped, and then polyadenylated by Poly(A) Tailing Kit (Thermo Fisher).

Luciferase assay

Five oocytes were collected per aliquot, and Nano-Glo Dual-Luciferase Reporter Assay System (Promega, cat# N1610) was used to measure the samples as per the manufacturer's protocol.

2'-OH methylation assay

Oligonucleotides or oocytes (supplemented with a methylated miR-221 oligonucleotide as an internal normalization control) were incubated in 50 μl Borax buffer with sodium periodate for 30 min at room temperature in dark. Next, 3 μl of 60% glycerol was added and further incubated for 10 min at RT. This was followed by

© 2021 The Authors

phenol–chloroform extraction and precipitation with isopropanol. The pellet was dissolved in water and used for cDNA synthesis followed by qPCR, which was set in technical triplicates for each biological sample (also in triplicates). Average CT values were first normalized to internal methylated miR-221 control followed by normalization to untreated sample.

ssc-miR-205 predicted target selection

To identify putative *ssc-miR-205* targets, we used sequences of 3'UTRs of all annotated porcine genes and counted the presence of complementary sequences to *ssc-mir-205 seeds* (seed 6mer UGAAGG, seed 7mer_m8 AUGAAGG, seed 8mer AUGAAGGA, and seed 7mer_1a UGAAGGA). From the top-scoring genes with most seed matches, we selected four targets based on low but well detectable expression in RNA-seq data from porcine oocytes (Gad *et al*, 2019). The rationale for this criterion was that miRNA targets would be expected to have reduced expression. Each of the selected putative targets had seven to nine 6mers and two to four 7mers (Table EV2). In addition, we included *Plcb1* among the putative targets as a candidate conserved target because it was the best predicted *mmu-miR-205* target by TargetScanVert in miRBase (Kozomara *et al*, 2019) and its porcine transcript carried one conserved 8mer binding site plus an additional 6mer (Table EV2).

Analysis of high-throughput sequencing data

Small RNA-sequencing data from mouse (GSE59254 (Garcia-Lopez *et al*, 2015)), porcine (GSE122032 (Gad *et al*, 2019)), and bovine (GSE 64942 (Roovers *et al*, 2015)) oocytes were mapped to their respective genomes (mouse—mm10, cow—bosTau9, pig—susScr11) as described previously (Demeter *et al*, 2019). After mapping, 21- to 23-nt-long reads perfectly aligned to the genome were selected for mature miRNA expression quantification with annotation from miRBase (Kozomara *et al*, 2019) using featureCounts v2.0.0 program (Liao *et al*, 2014):

```
featureCounts -a miRBase.${GENOME}.gff3 -o
${FILE}.counts.txt ${FILE}.bam -T 12 -F GTF --
fracOverlap 0.75 -f -t miRNA -g ID -M -O --fraction
```

For bovine and porcine samples, miRBase annotation was lifted over from older genome versions using Liftoff (Shumate & Salzberg, 2020).

Long RNA-seq data from mouse (GSE116771 (Horvat *et al*, 2018)), porcine (PRJNA548212 (Jiao *et al*, 2020)), and bovine (GSE52415 (Graf *et al*, 2014)) fully grown oocytes were mapped to their respective genomes (mouse—mm10, cow—bosTau9, pig—susScr11) using STAR 2.5.3a (Dobin *et al*, 2013) as previously described (Horvat *et al*, 2018).

Read mapping coverage was visualized in the UCSC Genome Browser by constructing bigWig tracks from merged replicates using the UCSC tools (Kent *et al*, 2010).

Data availability

No primary RNA-seq datasets have been generated and deposited.

Expanded View for this article is available online.

Acknowledgements
We thank Radek Malik for help with preparation of the manuscript. This work was funded by the European Research Council under the European Union's Horizon 2020 Research and Innovation Programme (Grant Agreement No. 647403, D-FENS). IMG institutional support included RVO: 68378050-KAV-NPUI. J.K. and V.K. were in part supported by IAPG institutional support RVO: 67985904. Computational resources for F.H. were supported by the European Structural and Investment Funds Grant (#KK.01.1.1.01.0010) and the Croatian National Centre of Research Excellence for Data Science and Advanced Cooperative Systems (#KK.01.1.1.01.0009). Financial support of S.K., F.H., and M.I.R.K. was in part provided by the Charles University in Prague in the form of a PhD student fellowship; this work will be in part used to fulfill the requirements for a PhD degree and hence can be considered "school work".

Author contributions
SK, VK, and MIRK performed the experiments. FH analyzed RNA-sequencing data. SK, JK, and PS designed the experiments, supervised, and analyzed experimental data. SK and PS wrote the manuscript.

Conflict of interest
The authors declare that they have no conflict of interest.

References

Abe K, Yamamoto R, Franke V, Cao M, Suzuki Y, Suzuki MG, Vlahovicek K, Svoboda P, Schultz RM, Aoki F (2015) The first murine zygotic transcription is promiscuous and uncoupled from splicing and 3' processing. *EMBO J* 34: 1523 – 1537

Appeltant R, Beek J, Vandenberghe L, Maes D, Van Soom A (2015) Increasing the cAMP concentration during in vitro maturation of pig oocytes improves cumulus maturation and subsequent fertilization in vitro. *Theriogenology* 83: 344 – 352

Bartel DP (2018) Metazoan microRNAs. *Cell* 173: 20 – 51

Bishop JO, Morton JG, Rosbash M, Richardson M (1974) Three abundance classes in HeLa cell messenger RNA. *Nature* 250: 199 – 204

Blaha M, Nemcova L, Kepkova KV, Vodicka P, Prochazka R (2015) Gene expression analysis of pig cumulus-oocyte complexes stimulated *in vitro* with follicle stimulating hormone or epidermal growth factor-like peptides. *Reprod Biol Endocrinol* 13: 113

Bosson AD, Zamudio JR, Sharp PA (2014) Endogenous miRNA and target concentrations determine susceptibility to potential ceRNA competition. *Mol Cell* 56: 347 – 359

Brennecke J, Stark A, Russell RB, Cohen SM (2005) Principles of microRNA-target recognition. *PLoS Biol* 3: e85

Brower PT, Gizang E, Boreen SM, Schultz RM (1981) Biochemical studies of mammalian oogenesis: synthesis and stability of various classes of RNA during growth of the mouse oocyte *in vitro*. *Dev Biol* 86: 373 – 383

Carter MG, Sharov AA, VanBuren V, Dudekula DB, Carmack CE, Nelson C, Ko MS (2005) Transcript copy number estimation using a mouse whole-genome oligonucleotide microarray. *Genome Biol* 6: R61

Chekulaeva M, Mathys H, Zipprich JT, Attig J, Colic M, Parker R, Filipowicz W (2011) miRNA repression involves GW182-mediated recruitment of CCR4-NOT through conserved W-containing motifs. *Nat Struct Mol Biol* 18: 1218 – 1226

Chen L, Hu X, Dai Y, Li Q, Wang X, Li Q, Xue K, Li Y, Liang J, Wang Y *et al* (2012) MicroRNA-27a activity is not suppressed in porcine oocytes. *Front Biosci* 4: 2679 – 2685

 © 2021 The Authors

Chen Y, Boland A, Kuzuoglu-Ozturk D, Bawankar P, Loh B, Chang CT, Weichenrieder O, Izaurralde E (2014) A DDX6-CNOT1 complex and W-binding pockets in CNOT9 reveal direct links between miRNA target recognition and silencing. *Mol Cell* 54: 737 – 750

D'Ambrogio A, Gu W, Udagawa T, Mello CC, Richter JD (2012) Specific miRNA stabilization by Gld2-catalyzed monoadenylation. *Cell Rep* 2: 1537 – 1545

De Leon V, Johnson A, Bachvarova R (1983) Half-lives and relative amounts of stored and polysomal ribosomes and poly(A) + RNA in mouse oocytes. *Dev Biol* 98: 400 – 408

Demeter T, Vaskovicova M, Malik R, Horvat F, Pasulka J, Svobodova E, Flemr M, Svoboda P (2019) Main constraints for RNAi induced by expressed long dsRNA in mouse cells. *Life Sci Alliance* 2: e201800289

Denzler R, Agarwal V, Stefano J, Bartel DP, Stoffel M (2014) Assessing the ceRNA hypothesis with quantitative measurements of miRNA and target abundance. *Mol Cell* 54: 766 – 776

Denzler R, McGeary SE, Title AC, Agarwal V, Bartel DP, Stoffel M (2016) Impact of microRNA levels, target-site complementarity, and cooperativity on competing endogenous RNA-regulated gene expression. *Mol Cell* 64: 565 – 579

Dobin A, Davis CA, Schlesinger F, Drenkow J, Zaleski C, Jha S, Batut P, Chaisson M, Gingeras TR (2013) STAR: ultrafast universal RNA-seq aligner. *Bioinformatics* 29: 15 – 21

Doench JG, Petersen CP, Sharp PA (2003) siRNAs can function as miRNAs. *Genes Dev* 17: 438 – 442

England CG, Ehlerding EB, Cai W (2016) NanoLuc: a small luciferase is brightening up the field of bioluminescence. *Bioconjug Chem* 27: 1175 – 1187

Fan X, Zhang X, Wu X, Guo H, Hu Y, Tang F, Huang Y (2015) Single-cell RNA-seq transcriptome analysis of linear and circular RNAs in mouse preimplantation embryos. *Genome Biol* 16: 148

Freimer JW, Krishnakumar R, Cook MS, Blelloch R (2018) Expression of alternative Ago2 isoform associated with loss of microRNA-driven translational repression in mouse oocytes. *Curr Biol* 28: 296 – 302

Friedman RC, Farh KK, Burge CB, Bartel DP (2009) Most mammalian mRNAs are conserved targets of microRNAs. *Genome Res* 19: 92 – 105

Fuchs Wightman F, Giono LE, Fededa JP, de la Mata M (2018) Target RNAs strike back on microRNAs. *Front Genet* 9: 435

Gad A, Nemcova L, Murin M, Kanka J, Laurincik J, Benc M, Pendovski L, Prochazka R (2019) microRNA expression profile in porcine oocytes with different developmental competence derived from large or small follicles. *Mol Reprod Dev* 86: 426 – 439

Gad A, Murin M, Nemcova L, Bartkova A, Laurincik J, Prochazka R (2020) Inhibition of miR-152 during *in vitro* maturation enhances the developmental potential of porcine embryos. *Animals* 10: 2289

Garcia-Lopez J, Alonso L, Cardenas DB, Artaza-Alvarez H, Hourcade Jde D, Martinez S, Brieno-Enriquez MA, Del Mazo J (2015) Diversity and functional convergence of small noncoding RNAs in male germ cell differentiation and fertilization. *RNA* 21: 946 – 962

Giraldez AJ, Mishima Y, Rihel J, Grocock RJ, Van Dongen S, Inoue K, Enright AJ, Schier AF (2006) Zebrafish MiR-430 promotes deadenylation and clearance of maternal mRNAs. *Science* 312: 75 – 79

Graf A, Krebs S, Zakhartchenko V, Schwalb B, Blum H, Wolf E (2014) Fine mapping of genome activation in bovine embryos by RNA sequencing. *Proc Natl Acad Sci USA* 111: 4139 – 4144

Griffin J, Emery BR, Huang I, Peterson CM, Carrell DT (2006) Comparative analysis of follicle morphology and oocyte diameter in four mammalian species (mouse, hamster, pig, and human). *J Exp Clin Assist Reprod* 3: 2

Hastie ND, Bishop JO (1976) The expression of three abundance classes of messenger RNA in mouse tissues. *Cell* 9: 761 – 774

He L, Thomson JM, Hemann MT, Hernando-Monge E, Mu D, Goodson S, Powers S, Cordon-Cardo C, Lowe SW, Hannon GJ *et al* (2005) A microRNA polycistron as a potential human oncogene. *Nature* 435: 828 – 833

Horvat F, Fulka H, Jankele R, Malik R, Jun M, Solcova K, Sedlacek R, Vlahovicek K, Schultz RM, Svoboda P (2018) Role of Cnot6l in maternal mRNA turnover. *Life Sci Alliance* 1: e201800084

Hutvagner G, Zamore PD (2002) A microRNA in a multiple-turnover RNAi enzyme complex. *Science* 297: 2056 – 2060

Hwang IS, Park MR, Lee HS, Kwak TU, Son HY, Kang JK, Lee JW, Lee K, Park EW, Hwang S (2020) Developmental and degenerative characterization of porcine parthenogenetic fetuses during early pregnancy. *Animals* 10: 622

Jahn CL, Baran MM, Bachvarova R (1976) Stability of RNA synthesized by the mouse oocyte during its major growth phase. *J Exp Zool* 197: 161 – 171

Jiao Y, Gao B, Wang G, Li H, Ahmed JZ, Zhang D, Ye S, Liu S, Li M, Shi D *et al* (2020) The key long non-coding RNA screening and validation between germinal vesicle and metaphase II of porcine oocyte in vitro maturation. *Reprod Domest Anim* 55: 351 – 363

Jinek M, Doudna JA (2009) A three-dimensional view of the molecular machinery of RNA interference. *Nature* 457: 405 – 412

Kataruka S, Modrak M, Kinterova V, Malik R, Zeitler DM, Horvat F, Kanka J, Meister G, Svoboda P (2020) MicroRNA dilution during oocyte growth disables the microRNA pathway in mammalian oocytes. *Nucleic Acids Res* 48: 8050 – 8062

Kent WJ, Zweig AS, Barber G, Hinrichs AS, Karolchik D (2010) BigWig and BigBed: enabling browsing of large distributed datasets. *Bioinformatics* 26: 2204 – 2207

Kim VN, Han J, Siomi MC (2009) Biogenesis of small RNAs in animals. *Nat Rev* 10: 126 – 139

Kinterova V, Kanka J, Petruskova V, Toralova T (2019) Inhibition of Skp1-Cullin-F-box complexes during bovine oocyte maturation and preimplantation development leads to delayed development of embryos. *Biol Reprod* 100: 896 – 906

Kozomara A, Birgaoanu M, Griffiths-Jones S (2019) miRBase: from microRNA sequences to function. *Nucleic Acids Res* 47: D155 – D162

Krol J, Loedige I, Filipowicz W (2010) The widespread regulation of microRNA biogenesis, function and decay. *Nat Rev Genet* 11: 597 – 610

Krutzfeldt J, Rajewsky N, Braich R, Rajeev KG, Tuschl T, Manoharan M, Stoffel M (2005) Silencing of microRNAs *in vivo* with 'antagomirs'. *Nature* 438: 685 – 689

Liang H, Jiao Z, Rong W, Qu S, Liao Z, Sun X, Wei Y, Zhao Q, Wang J, Liu Y *et al* (2020) 3'-Terminal 2'-O-methylation of lung cancer miR-21-5p enhances its stability and association with Argonaute 2. *Nucleic Acids Res* 48: 7027 – 7040

Liao Y, Smyth GK, Shi W (2014) featureCounts: an efficient general purpose program for assigning sequence reads to genomic features. *Bioinformatics* 30: 923 – 930

Lim LP, Glasner ME, Yekta S, Burge CB, Bartel DP (2003) Vertebrate microRNA genes. *Science* 299: 1540

Liu J, Carmell MA, Rivas FV, Marsden CG, Thomson JM, Song JJ, Hammond SM, Joshua-Tor L, Hannon GJ (2004) Argonaute2 is the catalytic engine of mammalian RNAi. *Science* 305: 1437 – 1441

Liu Y, Zhu Z, Ho IHT, Shi Y, Li J, Wang X, Chan MTV, Cheng CHK (2020) Genetic deletion of miR-430 disrupts maternal-zygotic transition and embryonic body plan. *Front Genet* 11: 853

Ma J, Flemr M, Stein P, Berninger P, Malik R, Zavolan M, Svoboda P, Schultz RM (2010) MicroRNA activity is suppressed in mouse oocytes. *Curr Biol* 20: 265 – 270

© 2021 The Authors

Marinov GK, Williams BA, McCue K, Schroth GP, Gertz J, Myers RM, Wold BJ (2014) From single-cell to cell-pool transcriptomes: stochasticity in gene expression and RNA splicing. *Genome Res* 24: 496 – 510

Meister G, Landthaler M, Patkaniowska A, Dorsett Y, Teng G, Tuschl T (2004) Human Argonaute2 mediates RNA cleavage targeted by miRNAs and siRNAs. *Mol Cell* 15: 185 – 197

Nishihara T, Zekri L, Braun JE, Izaurralde E (2013) miRISC recruits decapping factors to miRNA targets to enhance their degradation. *Nucleic Acids Res* 41: 8692 – 8705

Piko L, Clegg KB (1982) Quantitative changes in total RNA, total poly(A), and ribosomes in early mouse embryos. *Dev Biol* 89: 362 – 378

Piwecka M, Glažar P, Hernandez-Miranda LR, Memczak S, Wolf SA, Rybak-Wolf A, Filipchyk A, Klironomos F, Cerda Jara CA, Fenske P *et al* (2017) Loss of a mammalian circular RNA locus causes miRNA deregulation and affects brain function. *Science* 357: eaam8526

Prather RS (1993) Nuclear control of early embryonic development in domestic pigs. *J Reprod Fertil Suppl* 48: 17 – 29

Roovers EF, Rosenkranz D, Mahdipour M, Han CT, He N, de Sousa C, Lopes SM, van der Westerlaken LA, Zischler H, Butter F *et al* (2015) Piwi proteins and piRNAs in mammalian oocytes and early embryos. *Cell Rep* 10: 2069 – 2082

Rouya C, Siddiqui N, Morita M, Duchaine TF, Fabian MR, Sonenberg N (2014) Human DDX6 effects miRNA-mediated gene silencing via direct binding to CNOT1. *RNA* 20: 1398 – 1409

Salomon WE, Jolly SM, Moore MJ, Zamore PD, Serebrov V (2015) Single-molecule imaging reveals that argonaute reshapes the binding properties of its nucleic acid guides. *Cell* 162: 84 – 95

Schmitter D, Filkowski J, Sewer A, Pillai RS, Oakeley EJ, Zavolan M, Svoboda P, Filipowicz W (2006) Effects of Dicer and Argonaute down-regulation on mRNA levels in human HEK293 cells. *Nucleic Acids Res* 34: 4801 – 4815

Sheu-Gruttadauria J, Pawlica P, Klum SM, Wang S, Yario TA, Schirle Oakdale NT, Steitz JA, MacRae IJ (2019) Structural basis for target-directed microRNA degradation. *Mol Cell* 75: 1243 – 1255

Shumate A, Salzberg SL (2020) Liftoff: accurate mapping of gene annotations. *Bioinformatics* 37: 1639 – 1643

Sinha PB, Tesfaye D, Rings F, Hossien M, Hoelker M, Held E, Neuhoff C, Tholen E, Schellander K, Salilew-Wondim D (2017) MicroRNA-130b is involved in bovine granulosa and cumulus cells function, oocyte maturation and blastocyst formation. *J Ovarian Res* 10: 37

Sollner JF, Leparc G, Hildebrandt T, Klein H, Thomas L, Stupka E, Simon E (2017) An RNA-Seq atlas of gene expression in mouse and rat normal tissues. *Sci Data* 4: 170185

Sontheimer EJ (2005) Assembly and function of RNA silencing complexes. *Nat Rev* 6: 127 – 138

Su H, Trombly MI, Chen J, Wang XZ (2009) Essential and overlapping functions for mammalian Argonautes in microRNA silencing. *Genes Dev* 23: 304 – 317

Suh N, Baehner L, Moltzahn F, Melton C, Shenoy A, Chen J, Blelloch R (2010) MicroRNA function is globally suppressed in mouse oocytes and early embryos. *Curr Biol* 20: 271 – 277

Svoboda P, Franke V, Schultz RM (2015) Sculpting the transcriptome during the oocyte-to-embryo transition in mouse. *Curr Top Dev Biol* 113: 305 – 349

Veselovska L, Smallwood SA, Saadeh H, Stewart KR, Krueger F, Maupetit-Mehouas S, Arnaud P, Tomizawa S, Andrews S, Kelsey G (2015) Deep sequencing and de novo assembly of the mouse oocyte transcriptome define the contribution of transcription to the DNA methylation landscape. *Genome Biol* 16: 209

Wang WH, Abeydeera LR, Okuda K, Niwa K (1994) Penetration of porcine oocytes during maturation *in vitro* by cryopreserved, ejaculated spermatozoa. *Biol Reprod* 50: 510 – 515

Wang TY, Zhang J, Zhu J, Lian HY, Yuan HJ, Gao M, Luo MJ, Tan JH (2017) Expression profiles and function analysis of microRNAs in postovulatory aging mouse oocytes. *Aging* 9: 1186 – 1201

Wee LM, Flores-Jasso CF, Salomon WE, Zamore PD (2012) Argonaute divides its RNA guide into domains with distinct functions and RNA-binding properties. *Cell* 151: 1055 – 1067

Yang Q, Lin J, Liu M, Li R, Tian B, Zhang X, Xu B, Liu M, Zhang X, Li Y *et al* (2016) Highly sensitive sequencing reveals dynamic modifications and activities of small RNAs in mouse oocytes and early embryos. *Sci Adv* 2: e1501482

Yekta S, Shih IH, Bartel DP (2004) MicroRNA-directed cleavage of HOXB8 mRNA. *Science* 304: 594 – 596

License: This is an open access article under the terms of the Creative Commons Attribution-NonCommercial-NoDerivs License, which permits use and distribution in any medium, provided the original work is properly cited, the use is non-commercial and no modifications or adaptations are made.